ACS APPLIED ENERGY MATERIALS

www.acsaem.org Article

Efficient and Stable $FAPbBr_3$ Perovskite Solar Cells via Interface Modification by a Low-Dimensional Perovskite Layer

Yawen Liu, Byeong Jo Kim, Hua Wu, Gerrit Boschloo, and Erik M. J. Johansson*

Cite This: *ACS Appl. Energy Mater.* 2021, 4, 9276−9282 Read Online

ACCESS | Metrics & More | Article Recommendations | Supporting Information

ABSTRACT: Lead bromide perovskite with high bandgap and good stability has aroused broad interest for utilization in perovskite solar cells (PSCs) with high photovoltage, especially as a candidate for the front cell of tandem solar cells. However, the efficiency of lead bromide PSCs is still much lower than the standard lead iodide PSCs, and the defects in the perovskite are one of the main limiting factors hindering device performance. The construction of a 2D/3D perovskite interface is an effective way to passivate the interfacial defects and achieve efficient and stable PSCs. Herein, a facile and effective phenethylammonium bromide (PEABr) treatment method was applied to build a 2D/3D perovskite interface in $FAPbBr_3$ solar cells. An ultrathin layer of 2D PEA_2PbBr_4 perovskite was successfully fabricated on the surface of 3D $FAPbBr_3$ perovskite by depositing the PEABr solution on the 3D perovskite films. The 2D perovskite layer significantly passivated the interfacial defects, leading to enhancement of power conversion efficiency from 7.7% to 9.4% and fill factor from 67.6% to 77.6%. Moreover, the hydrophobic alkyl chain in the PEA cation improved the moisture tolerance of the perovskite and significantly increases the solar cell stability. Additionally, the PEABr treatment strategy was successfully utilized for preparing semitransparent 2D/3D $FAPbBr_3$ perovskite solar cells.

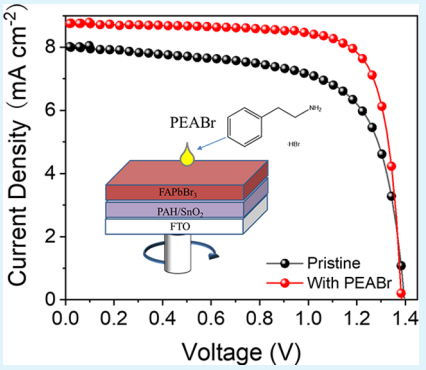

KEYWORDS: *high bandgap perovskite solar cells, PEABr, $FAPbBr_3$, 2D/3D perovskite, passivation*

INTRODUCTION

Over the past decade, significant progress has been achieved for perovskite solar cells (PSCs) with the highest power conversion efficiency (PCE) now exceeding 25%.[1−4] Among the various of perovskite materials, lead bromide perovskite[5−7] has recently attracted great attention as an interesting candidate for the top cell of tandem devices, benefiting from its high bandgap (around 2.3 eV), high V_{oc}, and good chemical stability in ambient air.[8−10] Hanusch et al. first reported $FAPbBr_3$ solar cells with a PCE of 6.5%.[11] Arora et al. and Chen et al. improved the quality of perovskite films via two-step[12] and one-step[13] solvent engineering, respectively. Zhang et al. obtained high-quality $FAPbBr_3$ films by adding the appropriate amount of urea in $FAPbBr_3$.[7] According to the detailed analysis of the single-junction $FAPbBr_3$ solar cells, the maximum efficiency of this kind of device is about 17%. However, until now, the efficiency of $FAPbBr_3$ is still far from its limit due to energy loss.[14]

The defects on the grain boundaries or the surface (interface defects), which were generated due to the sublimation of the organic components during thermal annealing, are one of the main limiting factors hindering device performance.[15−17] It is well recognized that the charge recombination caused by defects would lead to a decrease of fill factor (FF)[18] and a decrease of photovoltage. Moreover, interfacial defects also lead to severe hysteresis due to the ion migration and lifetime degradation as a result of the accumulation of moisture at the interface defects.[16,19−21]

Extensive research strategies related to defect passivation have been exploited to alleviate the above drawbacks.[22−25] In particular, Paek and co-workers reduced the surface defects by preparing two-dimensional (2D) perovskite on three-dimensional (3D) mixed perovskite films, increasing the PCE to 21.65%.[26] The organic spacer cations in low dimensional perovskite are usually hydrophobic. Therefore, low dimensional perovskite commonly has a stronger resistance to water induced degradation than 3D perovskite.[27,28] In addition, the 2D perovskite can coordinate to the surface of the 3D perovskite surface, thereby significantly reducing the defect density and improving the interfacial charge extraction efficiency.[29−31] Thus, by interfacial modification using a low-dimensional perovskite thin layer on the 3D perovskite, the efficiency as well as stability of the devices may be significantly improved.

Herein, we introduce a simple method to form a 2D/3D heterojunction structure to passivate the defects on the surface

Received: May 27, 2021
Published: September 16, 2021

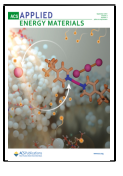

https://doi.org/10.1021/acsaem.1c01512
ACS Appl. Energy Mater. 2021, 4, 9276−9282

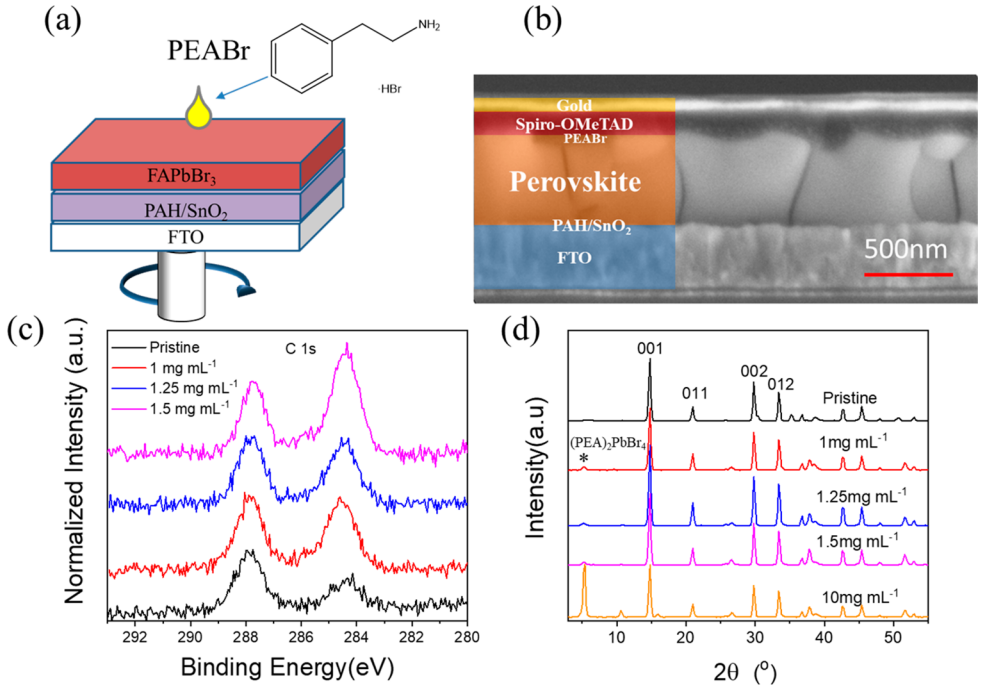

Figure 1. (a) The schematic structure and diagram of the 2D perovskite layer preparation on the 3D lead bromide perovskite. (b) The cross-sectional view of the device with 2D perovskite layer. (c) X-ray photoelectron spectroscopy (XPS) and (d) X-ray diffraction (XRD) for the perovskite films with and without surface modification with 2D perovskite prepared using different concentrations of PEABr.

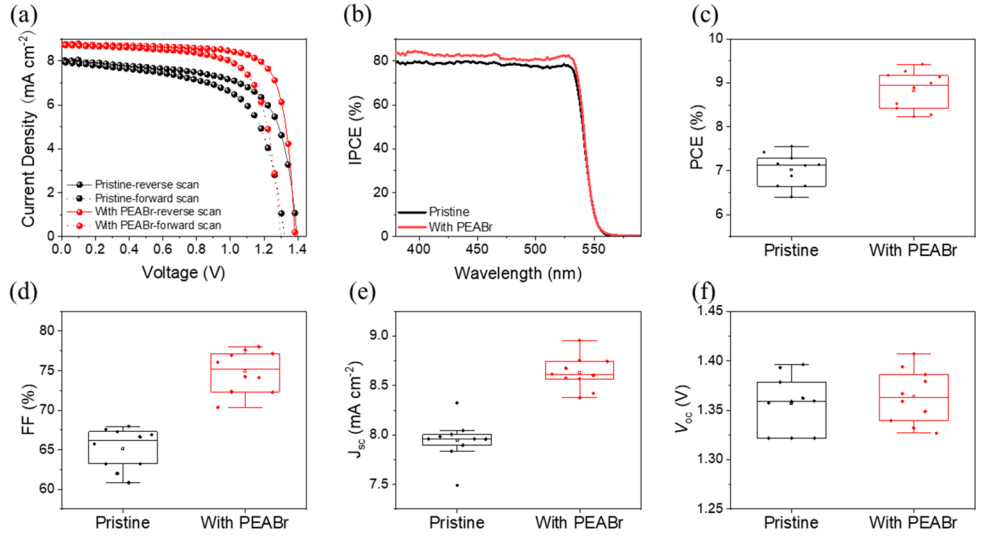

Figure 2. (a) Current density−voltage curves (J−V) and (b) incident photon-to-current efficiency (IPCE) spectra for the best performance devices without and with PEABr. The concentration of the PEABr is 1.25 mg mL^{-1}. Photovoltaic parameters for the devices without and with PEABr (10 devices), including (c) PCE, (d) FF, (e) short-circuit current density (J_{sc}), and (f) V_{oc}.

of $FAPbBr_3$. The phenethylammonium bromide (PEABr) solution is deposited on the 3D perovskite and then an ultrathin 2D PEA_2PbBr_4 perovskite is formed. The PEABr exhibits passivation ability as implied by increased steady-state photoluminescence and decreased trap-state density (n_{trap}), resulting in a higher FF than the pristine device (77.6% compared to 67.6%, respectively). The champion efficiency of the device treated with PEABr is as high as 9.4%. In addition to the outstanding PV performance, the 2D perovskite formed at the surface and grain boundaries of $FAPbBr_3$ protects the $FAPbBr_3$ from moisture and ion migration by passivating the interface defects, leading to the improvement of the device stability. The device with PEABr still retained over 91% of its initial efficiency after 100 days. To demonstrate the potentials of PEABr treated $FAPbBr_3$ in semitransparent devices with PCE of 8.7% were successfully fabricated by reducing the thickness of gold from 80 to 15 nm. This may be interesting for use in applications with semitransparent solar cells with high photovoltage, or as a front cell in a tandem solar cell.

RESULTS AND DISCUSSION

The two-step spin-coated 3D lead bromide perovskite films were treated with PEABr solution without thermal annealing to introduce 2D perovskite on the 3D FAPbBr perovskite (Figure

https://doi.org/10.1021/acsaem.1c01512
ACS Appl. Energy Mater. 2021, 4, 9276−9282

Table 1. Photovoltaic Parameters for the Best Performance Devices without and with PEABr Surface Modification

devices	scan direction	PCE (%)	FF (%)	J_{sc} (mA·cm^{-2})	V_{oc} (V)	R_{sh} (Ω·cm^2)	R_{s1} (Ω·cm^2)
pristine	reverse	7.6	67.6	8.0	1.39	2605	9
	forward	6.6	63.2	8.0	1.32	1056	15.5
	average	7.0 ± 0.7	65.3 ± 4	8.0 ± 0.4	1.39 ± 0.1	3000	12
with PEABr	reverse	9.4	77.6	8.8	1.39	6306	5
	forward	8.2	72.1	8.7	1.33	3434	9.5
	average	8.8 ± 0.6	74.9 ± 4	8.6 ± 0.3	1.40 ± 0.1	9666	7

1a, please find the fabrication details in the Supporting Information, SI). The PSC devices treated with PEABr concentrations from 0 mg mL^{-1} to 1.5 mg mL^{-1} were fabricated to optimize the concentration of PEABr solution for the 2D perovskite layer formation.

The structure of the PSC was confirmed by scanning electron microscope (SEM), as shown in Figure 1b, the thickness of the $FAPbBr_3$ film was around 500 nm and the cross-section structure of glass/FTO/PAH-SnO_2/3D-$FAPbBr_3$ perovskite/2D-perovskite/spiro-MeOTAD/Au was monitored.

The surface of the perovskite films was examined by using X-ray Photoelectron spectroscopy (XPS). The high-resolution XPS spectra of C 1s showed peaks centered around 284.8 and 288 eV. The intensity of the signal at 284.8 eV increased with the addition of PEABr, which implied the existence of carbon-rich PEABr on the surface of the perovskite. The crystal structure of as-fabricated perovskite films was further measured using XRD. As shown in Figure 1d, an additional peak at an angle of approximately 5.2°, that is attributed to the 2D $(PEA)_2PbBr_4$ structure, could be detected after the PEABr treatment. The XRD pattern of pure PEA_2PbBr_4 in the Figure S2, and comparing to the XRD pattern of the $FAPbBr_3$ film treated with 10 mg mL^{-1} PEABr solution, the peak from 2D perovskite can be clearly observed, which proves the existence of the $(PEA)_2PbBr_4$ perovskite structure on the $FAPbBr_3$ films after the treatment of the PEABr.[25,32] XRD patterns with various incident angles (from the 2° to 5°) were also measured for the sample with PEABr (1.25 mg mL^{-1}). As shown in Figure S3, the characteristic peak of 2D composite (around 5.2°) disappeared when the incident angle increased to 5°. Thus, we conclude that the thickness of the 2D layer is just a few nanometers. For the main diffraction peaks of the $FAPbBr_3$ (located at 14.8° and 29.7°), after being treated with 1.25 mg mL^{-1} PEABr, the intensity was higher than that of other perovskite films, which indicate improved crystallinity of the perovskite films after the surface modification.

$FAPbBr_3$ PSCs treated with different concentration of PEABr solution were fabricated to optimize the concentration of the PEABr solution. As shown in Figures 2a and S4 and Tables 1 and S1, the optimal concentration is 1.25 mg mL^{-1}, which lead to the highest PCE.

The J–V curves for the devices without and with PEABr (1.25 mg mL^{-1}) modification are compared in Figure 2a, and the corresponding data are listed in Table 1. The pristine device showed a lower PCE of 7.6% at a reverse scan together with a J_{sc} of 8.0 mA cm^{-2}, V_{oc} of 1.4 V, and an FF of 67.6%, while the device with PEABr treatment demonstrated the higher PCE of 9.4% at a reverse scan with J_{sc} = 8.8 mA cm^{-2}, V_{oc} = 1.4 V, and FF = 77.6%. The SEM images of the perovskite films are shown in Figure 3, and the corresponding IPCE spectra of the cells are shown in Figure 4b. The device with PEABr treatment showed higher IPCE in almost all wavelengths from 350 to 550 nm when compared to the pristine device, showing that the photon to

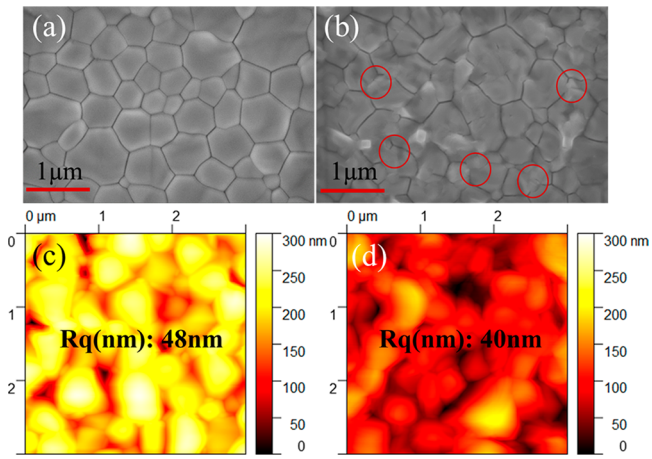

Figure 3. Scanning electron microscopy (SEM) images of the perovskite films (a) pristine and (b) with PEABr treatment. Red circles are examples of regions where differences are observed in the surface morphology. Atomic force microscopy (AFM) images of the perovskite films (c) pristine and (d) with PEABr treatment.

charge carrier conversion is enhanced after PEABr treatment to obtain the 2D perovskite interface. These results are in good agreement with the J–V curve, which showed that the PEABr-treated device has better photovoltaic performance than the pristine device. Figure 4 c–f monitors the PV parameter statistics of the devices with and without PEABr treatment. The results show that the PSCs showed good reproducibility in performance. Noticeably, from Tables 1 and S1, the FF of the devices improved significantly after the treatment of PEABr (from 67.6% to 77.6%), which contributed the most to the improvement of PCE.

The enhanced FF can be explained by changes in the losses connected to resistance in the device.[18,33] The resistance in the solar cells is often described as the series resistance (R_{s1}) and shunt resistance (R_{sh}), which are related to the materials, carrier recombination, and the contact between charge transport layer etc. In general, for a high FF, it is important to increase the R_{sh} and reduce the R_{s1}. From our results in Tables 1 and S1, the devices with PEABr treatment have higher R_{sh} and lower R_s than the pristine device, which leads to the higher FF and then the higher PCE.

To further understand the influence of the PEABr treatment on the perovskite films, SEM and AFM were performed to study the surface morphology of perovskite films. According to the SEM results in Figures 3a,b and S5, good perovskite films without pinholes could be obtained for all samples. There is no obvious difference in the particle size of the different perovskite films. But comparing the picture in Figure 3a,b, there are differences observed in the surface morphology indicating formation of a 2D perovskite interface for the sample with PEABr modification, which are consistent with the results of the

https://doi.org/10.1021/acsaem.1c01512
ACS Appl. Energy Mater. 2021, 4, 9276–9282

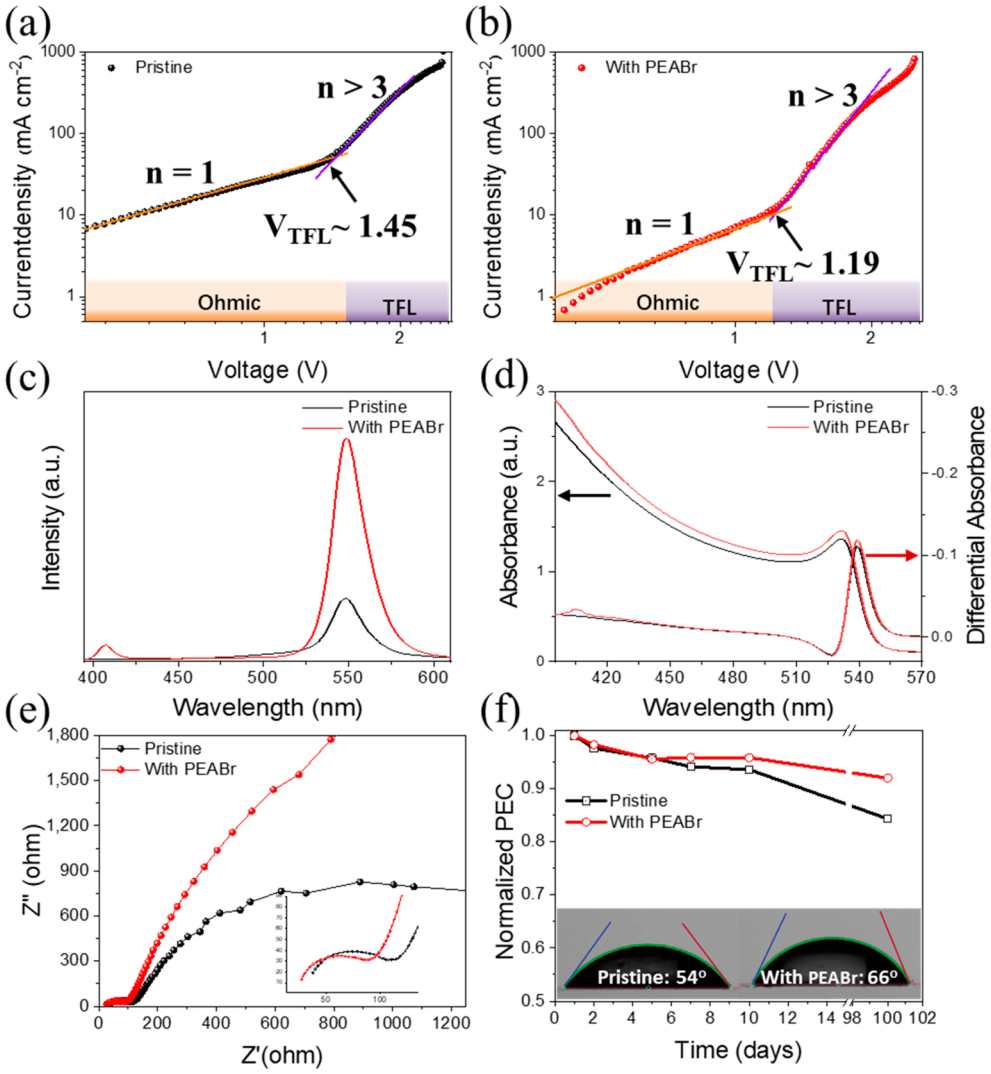

Figure 4. $J-V$ measurement of hole-only devices in the dark for determining the n_{trap}, (a) pristine and (b) with PEABr. The structure of the hole-only devices is (FTO/PEDOT: PSS/$FAPbBr_3$/ (with or without PEABr) /Spiro-OMeTAD/Au). (c) Steady-state photoluminescence and (d) UV−vis absorption spectra of the perovskite films with and without PEABr treatment, the structure of samples is glass/FTO/SnO_2/$FAPbBr_3$/with or without PEABr modification. (e) Nyquist plots of the PSCs devices with and without PEABr treatment. These devices were measured at 1.3 V under dark. (f) Long-term stability measurement of PSCs with and without PEABr modification. The inset in the image shows the water contact angle measurements for pristine and for PEABr modified perovskite films.

2D perovskite peaks detected in XRD. AFM was employed to obtain more information about the perovskite surface. From the images in Figures 3c,d, S6, and S7, the pristine perovskite film showed a rough surface morphology with a roughness of 48.0 nm. As shown in Figure 3d, the roughness of the perovskite treated with PEABr (1.25 mg mL^{-1}) is 40 nm, which therefore suggests a slightly improved smoothness of the PEABr modified film. When PEABr solutions with different concentrations were deposited on the perovskite films, the roughness change of the perovskite films was negligible. Low surface roughness facilitates the deposition of the HTM layers and reduces the interface resistance to accelerate the charge transport,[34] meanwhile a rough film with poor contact may cause pin holes, and therefore lower FF compared to a uniform film.[18]

The recombination of photogenerated electrons and holes, would lead to current leakage and, therefore, to reduced FF. An in-depth understanding of the role of 2D perovskite interface layer of the PEABr modified device and in the as-fabricated devices is important for the development of efficient PSC devices. Therefore, we analyzed the trap density (n_{trap}) of the perovskite films by employing the $J-V$ measurements under dark condition and for different bias voltages.[35] Generally, hole-only devices with the structure of FTO/PEDOT: PSS/perovskite/(with and without PEABr modification)/spiro-OMeTAD/Au were prepared. From the results shown in Figure 4a,b, there are two regions in the $J-V$ characteristic curves: Ohmic ($J \sim V^n$, $n = 1$, orange line) and trap-filled limit (TFL, $J \sim V^n$, $n > 3$, purple line) regions.[36,37] V_{TFL} is the trap-filled limit voltage, and it is determined by the trap states.[35,37,38] Thus, n_{trap} could be calculated by eq 1.[38]

$$n_{trap} = \frac{2\varepsilon_0 \varepsilon V_{TFL}}{eL^2} \quad (1)$$

where L is the thickness of the perovskite film (500 nm), ε_0 is the vacuum permittivity (8.854×10^{-12} F m^{-1}), and e is the elementary charge (1.602×10^{-19} C), the dielectric constants (ε) of $FAPbBr_3$ is 43.6.[39,40] As shown in Figure 4a,b, the calculated n_{trap} for the perovskite film with PEABr modification

https://doi.org/10.1021/acsaem.1c01512
ACS Appl. Energy Mater. 2021, 4, 9276−9282

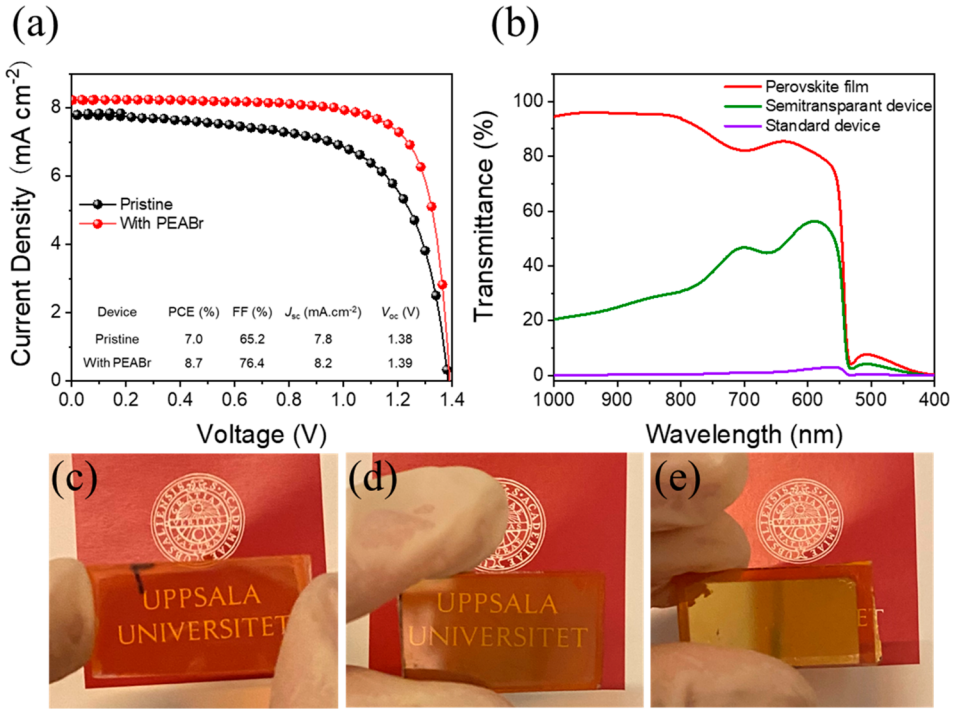

Figure 5. (a) $J-V$ curves of the champion semitransparent devices without and with PEABr modification. (b) The transmittance of the perovskite film, semitransparent PSCs, and the standard PSCs, all these samples were treated with PEABr. The thickness of Au for semitransparent device and standard device are 15 and 80 nm, respectively. The device pictures for the (c) perovskite film, (d) semitransparent device, and (e) standard device. University logo used with permission.

(2.3×10^{16} cm^{-3}) was slightly lower than that of pristine perovskite film (2.8×10^{16} cm^{-3}). The lower n_{trap} suggests a passivation effect by the 2D perovskite interface, as well as the improved perovskite quality previously discussed.[41]

As shown in Figures 4c and S8, in order to get the steady-state photoluminescence information on the whole standard devices, we performed a PL measurement for the devices with structure of glass/FTO/PAH-SnO_2/3D-$FAPbBr_3$ perovskite (with or without PEABr), as same time the perovskite films were also deposited on the glass directly with the structure of glass/3D-$FAPbBr_3$ perovskite (with or without PEABr) to avoid the possible quenching effect of electron transfer layer and get the intrinsic PL features of different perovskite layers. In both of the two cases, the PL intensity of the perovskite film with PEABr-modification was much higher than that of the pristine perovskite film, which also suggests reduced surface defects and better quality of the perovskite with the 2D perovskite interface. Moreover, the PEABr modified film showed a PL peak at 410 nm, which is related to the emission of the formed 2D $(PEA)_2PbBr_4$ perovskite.[32] The results are in good agreement with the XRD results and further confirmed the formation of 2D perovskite $(PEA)_2PbBr_4$ on the surface of $FAPbBr_3$. Moreover, as shown in Figure 4b, the UV−vis absorption spectra further confirmed the existence of this 2D perovskite. The differential curve shows the 405 nm absorption edge corresponding to the near-band edge transition in $(PEA)_2PbBr_4$.[32] In addition, the perovskite film with PEABr modification showed slightly enhanced absorption compared to the pristine perovskite, which may be the results of the improved crystallinity.[42] The enhanced light harvesting of sample with PEABr modification could be a reason for the improvement of J_{sc}.[43]

The resistance has a great influence on the FF of the device and is related to the charge transport and recombination in the device.[18,44] As shown in Figure 4e, electrochemical impedance spectroscopy (EIS) was applied to further understand how the PEABr modification affects the resistance of the device. The measurement was carried out under dark with an applied voltage of 1.3 V. The equivalent circuit in the Figure S9 included the series resistance (R_{s2}), charge transfer resistance (R_{ct}), and the recombination resistance (R_{recom}).[45,46] From Figure 4e and Table S2, after treatment, the R_{s2} was decreased from 34.33 to 25.95 Ω, and the R_{ct} value decreased from 76.57 to 67.30 Ω, while the R_{recom} increased from 3985 to 11128 Ω. The decreased series resistance for the device with PEABr treatment suggested a lower contact resistance between the $FAPbBr_3$ perovskite layer and HTL due to the presence of the 2D perovskite layer,[47] which is also consistent with the improved surface roughness in the AFM measurement. The smaller R_{ct} is good for the charge transfer.[47] Meanwhile, the device with PEABr modification showed higher R_{recom} in agreement with the lower defect density suggested by the PL measurements, which leads to an improved shunt resistance and enhanced FF.[47]

Interfacial defects can also reduce the lifetime of the device due to the accumulation of moisture at the interface defects.[16,19−21] From Figure 4f, owing to the original good stability of $FAPbBr_3$, the efficiency of pristine devices decreased only slightly after 100 days. With the protection of the hydrophobic organic spacer cation in PEABr, the PEABr modified device was more stable than the pristine device, and the PEABr modified device maintained 91% of its original efficiency after 100 days. The changes in hydrophobicity were verified by water contact angle measurements. As expected, the PEABr modified perovskite film showed the higher hydrophobicity than the pristine perovskite film (contact angle: 66° vs 54°), indicating a greater moisture stability.

https://doi.org/10.1021/acsaem.1c01512
ACS Appl. Energy Mater. 2021, 4, 9276−9282

Semitransparent solar cells may have many interesting areas of application and achieving a semitransparent device requires a highly transparent electrode. In this work, several semitransparent devices were prepared by reducing the thickness of gold from 80 to 15 nm. From the $J-V$ curves in Figure 5a and Figure S10, the photovoltaic performance of the semitransparent device (with 15 nm gold) is similar to the standard devices (with 80 nm gold). It is worth mentioning that the device with PEABr treatment showed a higher PCE (8.7%) than the pristine device without PEABr modification (7.0%). As shown in Figures 5b and S11, the transmittance of semitransparent PSCs and the standard PSCs films were measured. It is obvious that the semitransparent PSCs demonstrated a much higher transmittance than the standard PSCs. By reducing the thickness of the Au layer, the transparency was improved from 3% to 57%, with a peak in transmittance around 600 nm. The photos in Figure 5c–e also showed the same trend with the transmittance results. The successful construction of transparent devices showed that $FAPbBr_3$ solar cells has great potential and practical significance to be used in practical applications such as semitransparent windows or tandem solar cells in the future.

CONCLUSIONS

In summary, we have investigated the preparation and effect of interfacial modification of $FAPbBr_3$ with 2D PEA_2PbBr_4 perovskite, in solar cell devices. The 2D PEA_2PbBr_4 perovskite layer was formed by a surface modification using PEABr, which clearly improved the photovoltaic performance of our devices. For the interface modified devices the efficiency was improved from 7.7% to 9.4%, and the FF was improved from 67.7% to 77.6%, compared to the devices without 2D perovskite layer. With the 2D PEA_2PbBr_4 perovskite layer the intensity of steady-state photoluminescence also increased, which suggests that the trap density decreased. Moreover, the result of AFM and EIS suggest that the ultrathin 2D perovskite layer also helps to optimize the interface resistance between the perovskite and the HTL. The 2D perovskite layer also improves the stability of the devices by preventing moisture and oxygen from penetrating into the 3D perovskite. The champion device with PEABr treatment maintained 91% PCE after 100 days in the drybox and dark condition. Semitransparent devices with the 2D perovskite interface modification were also prepared and the champion PCE with interface modification was 8.7% with an FF up to 76.4%.

ASSOCIATED CONTENT

Supporting Information

The Supporting Information is available free of charge at https://pubs.acs.org/doi/10.1021/acsaem.1c01512.

Experimental details, SEM images, AFM images, $J-V$ curve, EIS parameters, SSPL spectra, equivalent circuit of model fitting for the impedance spectra, and transmittance spectra (PDF)

AUTHOR INFORMATION

Corresponding Author

Erik M. J. Johansson − *Department of Chemistry-Ångström, Physical Chemistry, Uppsala University, 75120 Uppsala, Sweden*; orcid.org/0000-0001-9358-8277; Email: erik.johansson@kemi.uu.se

Authors

Yawen Liu − *Department of Chemistry-Ångström, Physical Chemistry, Uppsala University, 75120 Uppsala, Sweden*

Byeong Jo Kim − *Department of Chemistry-Ångström, Physical Chemistry, Uppsala University, 75120 Uppsala, Sweden*

Hua Wu − *Department of Chemistry-Ångström, Physical Chemistry, Uppsala University, 75120 Uppsala, Sweden*

Gerrit Boschloo − *Department of Chemistry-Ångström, Physical Chemistry, Uppsala University, 75120 Uppsala, Sweden*; orcid.org/0000-0002-8249-1469

Complete contact information is available at: https://pubs.acs.org/10.1021/acsaem.1c01512

Notes

The authors declare no competing financial interest.

ACKNOWLEDGMENTS

The authors acknowledge the financial support obtained from the Swedish Energy Agency, ÅForsk, Swedish Research Council (VR), and Olle Engkvist Foundation. The research was also supported by Basic Science Research Program through the National Research Foundation of Korea (NRF) funded by the Ministry of Education (2020R1A6A3A03039130).

REFERENCES

(1) Kojima, A.; Teshima, K.; Shirai, Y.; Miyasaka, T. Organometal Halide Perovskites as Visible-Light Sensitizers for Photovoltaic Cells. *J. Am. Chem. Soc.* **2009**, *131* (17), 6050−6051.

(2) Lee, M. M.; Teuscher, J.; Miyasaka, T.; Murakami, T. N.; Snaith, H. J. Efficient Hybrid Solar Cells Based on Meso-Superstructured Organometal Halide Perovskites. *Science* **2012**, *338* (6107), 643−647.

(3) Jung, H. S.; Park, N. G. Perovskite Solar Cells: From Materials to Devices. *Small* **2015**, *11* (1), 10−25.

(4) https://www.nrel.gov/pv/cell-efficiency.html, Accessed August 31, 2021.

(5) Noh, J. H.; Im, S. H.; Heo, J. H.; Mandal, T. N.; Seok, S. I. Chemical Management for Colorful, Efficient, and Stable Inorganic−Organic Hybrid Nanostructured Solar Cells. *Nano Lett.* **2013**, *13* (4), 1764−1769.

(6) Edri, E.; Kirmayer, S.; Cahen, D.; Hodes, G. High Open-Circuit Voltage Solar Cells Based on Organic−Inorganic Lead Bromide Perovskite. *J. Phys. Chem. Lett.* **2013**, *4* (6), 897−902.

(7) Zhang, Y.; Liang, Y.; Wang, Y.; Guo, F.; Sun, L.; Xu, D. Planar FAPbBr3 Solar Cells with Power Conversion Efficiency above 10%. *ACS Energy Lett.* **2018**, *3* (8), 1808−1814.

(8) Albrecht, S.; Saliba, M.; Correa Baena, J. P.; Lang, F.; Kegelmann, L.; Mews, M.; Steier, L.; Abate, A.; Rappich, J.; Korte, L.; Schlatmann, R.; Nazeeruddin, M. K.; Hagfeldt, A.; Grätzel, M.; Rech, B. Monolithic perovskite/silicon-heterojunction tandem solar cells processed at low temperature. *Energy Environ. Sci.* **2016**, *9* (1), 81−88.

(9) Frost, J. M.; Butler, K. T.; Brivio, F.; Hendon, C. H.; van Schilfgaarde, M.; Walsh, A. Atomistic Origins of High-Performance in Hybrid Halide Perovskite Solar Cells. *Nano Lett.* **2014**, *14* (5), 2584−2590.

(10) Zheng, X.; Chen, B.; Yang, M.; Wu, C.; Orler, B.; Moore, R. B.; Zhu, K.; Priya, S. The Controlling Mechanism for Potential Loss in CH3NH3PbBr3 Hybrid Solar Cells. *ACS Energy Lett.* **2016**, *1* (2), 424−430.

(11) Hanusch, F. C.; Wiesenmayer, E.; Mankel, E.; Binek, A.; Angloher, P.; Fraunhofer, C.; Giesbrecht, N.; Feckl, J. M.; Jaegermann, W.; Johrendt, D.; Bein, T.; Docampo, P. Efficient Planar Heterojunction Perovskite Solar Cells Based on Formamidinium Lead Bromide. *J. Phys. Chem. Lett.* **2014**, *5* (16), 2791−2795.

(12) Arora, N.; Dar, M. I.; Hezam, M.; Tress, W.; Jacopin, G.; Moehl, T.; Gao, P.; Aldwayyan, A. S.; Deveaud, B.; Grätzel, M.; Nazeeruddin, M. K. Photovoltaic and Amplified Spontaneous Emission Studies of

High-Quality Formamidinium Lead Bromide Perovskite Films. *Adv. Funct. Mater.* **2016**, *26* (17), 2846−2854.
(13) Hu, C.; Shivarudraiah, S. B.; Sung, H. H. Y.; Williams, I. D.; Halpert, J. E.; Yang, S. Discovery of a New Intermediate Enables One-Step Deposition of High-Quality Perovskite Films via Solvent Engineering. *Solar RRL* **2021**, *5*, 2000712.
(14) Zohar, A.; Kulbak, M.; Levine, I.; Hodes, G.; Kahn, A.; Cahen, D. What Limits the Open-Circuit Voltage of Bromide Perovskite-Based Solar Cells? *ACS Energy Lett.* **2019**, *4* (1), 1−7.
(15) Yang, W. S.; Park, B.-W.; Jung, E. H.; Jeon, N. J.; Kim, Y. C.; Lee, D. U.; Shin, S. S.; Seo, J.; Kim, E. K.; Noh, J. H.; Seok, S. I. Iodide management in formamidinium-lead-halide−based perovskite layers for efficient solar cells. *Science* **2017**, *356* (6345), 1376−1379.
(16) Zheng, Y.; Yang, X.; Su, R.; Wu, P.; Gong, Q.; Zhu, R. High-Performance CsPbIxBr3-x All-Inorganic Perovskite Solar Cells with Efficiency over 18% via Spontaneous Interfacial Manipulation. *Adv. Funct. Mater.* **2020**, *30* (46), 2000457.
(17) Ball, J. M.; Petrozza, A. Defects in perovskite-halides and their effects in solar cells. *Nat. Energy* **2016**, *1* (11), 16149.
(18) Ma, C.; Park, N.-G. A Realistic Methodology for 30% Efficient Perovskite Solar Cells. *Chem.* **2020**, *6* (6), 1254−1264.
(19) Yang, D.; Yang, R.; Wang, K.; Wu, C.; Zhu, X.; Feng, J.; Ren, X.; Fang, G.; Priya, S.; Liu, S. High efficiency planar-type perovskite solar cells with negligible hysteresis using EDTA-complexed SnO2. *Nat. Commun.* **2018**, *9* (1), 3239.
(20) Kim, D. H.; Whitaker, J. B.; Li, Z.; van Hest, M. F. A. M.; Zhu, K. Outlook and Challenges of Perovskite Solar Cells toward Terawatt-Scale Photovoltaic Module Technology. *Joule* **2018**, *2* (8), 1437−1451.
(21) Chou, Y.-S.; Chou, L.-H.; Guo, A.-Z.; Wang, X.-F.; Osaka, I.; Wu, C.-G.; Liu, C.-L. Ultrasonic Spray-Coated Mixed Cation Perovskite Films and Solar Cells. *ACS Sustainable Chem. Eng.* **2019**, *7* (16), 14217−14224.
(22) Schulz, P.; Cahen, D.; Kahn, A. Halide Perovskites: Is It All about the Interfaces? *Chem. Rev.* **2019**, *119* (5), 3349−3417.
(23) Luo, D.; Su, R.; Zhang, W.; Gong, Q.; Zhu, R. Minimizing non-radiative recombination losses in perovskite solar cells. *Nat. Rev. Mater.* **2020**, *5* (1), 44−60.
(24) Chen, J.; Park, N.-G. Causes and Solutions of Recombination in Perovskite Solar Cells. *Adv. Mater.* **2019**, *31* (47), 1803019.
(25) Jiang, Q.; Zhao, Y.; Zhang, X.; Yang, X.; Chen, Y.; Chu, Z.; Ye, Q.; Li, X.; Yin, Z.; You, J. Surface passivation of perovskite film for efficient solar cells. *Nat. Photonics* **2019**, *13* (7), 460−466.
(26) Paek, S.; Roldán-Carmona, C.; Cho, K. T.; Franckevičius, M.; Kim, H.; Kanda, H.; Drigo, N.; Lin, K.-H.; Pei, M.; Gegevičius, R.; Yun, H. J.; Yang, H.; Schouwink, P. A.; Corminboeuf, C.; Asiri, A. M.; Nazeeruddin, M. K. Molecular Design and Operational Stability: Toward Stable 3D/2D Perovskite Interlayers. *Adv. Sci.* **2020**, *7* (19), 2001014.
(27) Lin, Y.; Bai, Y.; Fang, Y.; Chen, Z.; Yang, S.; Zheng, X.; Tang, S.; Liu, Y.; Zhao, J.; Huang, J. Enhanced Thermal Stability in Perovskite Solar Cells by Assembling 2D/3D Stacking Structures. *J. Phys. Chem. Lett.* **2018**, *9* (3), 654−658.
(28) Wang, Z.; Lin, Q.; Chmiel, F. P.; Sakai, N.; Herz, L. M.; Snaith, H. J. Efficient ambient-air-stable solar cells with 2D−3D heterostructured butylammonium-caesium-formamidinium lead halide perovskites. *Nat. Energy* **2017**, *2* (9), 17135.
(29) Bian, H.; Bai, D.; Jin, Z.; Wang, K.; Liang, L.; Wang, H.; Zhang, J.; Wang, Q.; Liu, S. Graded Bandgap CsPbI2+xBr1−x Perovskite Solar Cells with a Stabilized Efficiency of 14.4%. *Joule* **2018**, *2* (8), 1500−1510.
(30) Zheng, X.; Chen, B.; Dai, J.; Fang, Y.; Bai, Y.; Lin, Y.; Wei, H.; Zeng, X. C.; Huang, J. Defect passivation in hybrid perovskite solar cells using quaternary ammonium halide anions and cations. *Nat. Energy* **2017**, *2* (7), 17102.
(31) Tsai, H.; Nie, W.; Blancon, J.-C.; Stoumpos, C. C.; Asadpour, R.; Harutyunyan, B.; Neukirch, A. J.; Verduzco, R.; Crochet, J. J.; Tretiak, S.; Pedesseau, L.; Even, J.; Alam, M. A.; Gupta, G.; Lou, J.; Ajayan, P. M.; Bedzyk, M. J.; Kanatzidis, M. G.; Mohite, A. D. High-efficiency two-dimensional Ruddlesden−Popper perovskite solar cells. *Nature* **2016**, *536* (7616), 312−316.
(32) Zhang, Y.; Liu, Y.; Xu, Z.; Ye, H.; Li, Q.; Hu, M.; Yang, Z.; Liu, S. Two-dimensional (PEA)2PbBr4 perovskite single crystals for a high performance UV-detector. *J. Mater. Chem. C* **2019**, *7* (6), 1584−1591.
(33) Wang, Q.; Bi, C.; Huang, J. Doped hole transport layer for efficiency enhancement in planar heterojunction organolead trihalide perovskite solar cells. *Nano Energy* **2015**, *15*, 275−280.
(34) Wang, J.-F.; Zhu, L.; Zhao, B.-G.; Zhao, Y.-L.; Song, J.; Gu, X.-Q.; Qiang, Y.-H. Surface engineering of perovskite films for efficient solar cells. *Sci. Rep.* **2017**, *7* (1), 14478.
(35) Liu, Z.; Hu, J.; Jiao, H.; Li, L.; Zheng, G.; Chen, Y.; Huang, Y.; Zhang, Q.; Shen, C.; Chen, Q.; Zhou, H. Chemical Reduction of Intrinsic Defects in Thicker Heterojunction Planar Perovskite Solar Cells. *Adv. Mater.* **2017**, *29* (23), 1606774.
(36) Li, M.; Li, B.; Cao, G.; Tian, J. Monolithic MAPbI3 films for high-efficiency solar cells via coordination and a heat assisted process. *J. Mater. Chem. A* **2017**, *5* (40), 21313−21319.
(37) Shi, D.; Adinolfi, V.; Comin, R.; Yuan, M.; Alarousu, E.; Buin, A.; Chen, Y.; Hoogland, S.; Rothenberger, A.; Katsiev, K.; Losovyj, Y.; Zhang, X.; Dowben, P. A.; Mohammed, O. F.; Sargent, E. H.; Bakr, O. M. Low trap-state density and long carrier diffusion in organolead trihalide perovskite single crystals. *Science* **2015**, *347* (6221), 519−522.
(38) Liu, Y.; Yang, Z.; Cui, D.; Ren, X.; Sun, J.; Liu, X.; Zhang, J.; Wei, Q.; Fan, H.; Yu, F.; Zhang, X.; Zhao, C.; Liu, S. Two-Inch-Sized Perovskite CH3NH3PbX3 (X = Cl, Br, I) Crystals: Growth and Characterization. *Adv. Mater.* **2015**, *27* (35), 5176−5183.
(39) Han, Q.; Bae, S.-H.; Sun, P.; Hsieh, Y.-T.; Yang, Y.; Rim, Y. S.; Zhao, H.; Chen, Q.; Shi, W.; Li, G.; Yang, Y. Single Crystal Formamidinium Lead Iodide (FAPbI3): Insight into the Structural, Optical, and Electrical Properties. *Adv. Mater.* **2016**, *28* (11), 2253−2258.
(40) Zhumekenov, A. A.; Saidaminov, M. I.; Haque, M. A.; Alarousu, E.; Sarmah, S. P.; Murali, B.; Dursun, I.; Miao, X.-H.; Abdelhady, A. L.; Wu, T.; Mohammed, O. F.; Bakr, O. M. Formamidinium Lead Halide Perovskite Crystals with Unprecedented Long Carrier Dynamics and Diffusion Length. *ACS Energy Lett.* **2016**, *1* (1), 32−37.
(41) Liu, Y.; Liu, Z.; Lee, E.-C. Dimethyl-sulfoxide-assisted improvement in the crystallization of lead-acetate-based perovskites for high-performance solar cells. *J. Mater. Chem. C* **2018**, *6* (25), 6705−6713.
(42) Seol, D.-J.; Lee, J.-W.; Park, N.-G. On the Role of Interfaces in Planar-Structured HC(NH2)2PbI3 Perovskite Solar Cells. *ChemSusChem* **2015**, *8* (14), 2414−2419.
(43) Cao, X.; Li, C.; Li, Y.; Fang, F.; Cui, X.; Yao, Y.; Wei, J. Enhanced performance of perovskite solar cells by modulating the Lewis acid-base reaction. *Nanoscale* **2016**, *8* (47), 19804−19810.
(44) Sidhik, S.; Cerdan Pasarán, A.; Esparza, D.; López Luke, T.; Carriles, R.; De la Rosa, E. Improving the Optoelectronic Properties of Mesoporous TiO2 by Cobalt Doping for High-Performance Hysteresis-free Perovskite Solar Cells. *ACS Appl. Mater. Interfaces* **2018**, *10* (4), 3571−3580.
(45) Yang, L.; Cai, F.; Yan, Y.; Li, J.; Liu, D.; Pearson, A. J.; Wang, T. Conjugated Small Molecule for Efficient Hole Transport in High-Performance p-i-n Type Perovskite Solar Cells. *Adv. Funct. Mater.* **2017**, *27* (31), 1702613.
(46) Hsiao, K.-C.; Jao, M.-H.; Li, B.-T.; Lin, T.-H.; Liao, S. H.-C.; Wu, M.-C.; Su, W.-F. Enhancing Efficiency and Stability of Hot Casting p−i−n Perovskite Solar Cell via Dipolar Ion Passivation. *ACS Appl. Energy Mater.* **2019**, *2* (7), 4821−4832.
(47) Lv, Y.; Shi, Y.; Song, X.; Liu, J.; Wang, M.; Wang, S.; Feng, Y.; Jin, S.; Hao, C. Bromine Doping as an Efficient Strategy to Reduce the Interfacial Defects in Hybrid Two-Dimensional/Three-Dimensional Stacking Perovskite Solar Cells. *ACS Appl. Mater. Interfaces* **2018**, *10* (37), 31755−31764.

https://doi.org/10.1021/acsaem.1c01512
ACS Appl. Energy Mater. 2021, 4, 9276−9282